Scientific Research Publishing

Journal of Sensor Technology, 2023, 13, 37-50
https://www.scirp.org/journal/jst
ISSN Online: 2161-1238
ISSN Print: 2161-122X

Personnel Localization of Real-Time Kinematic Based on Pedestrian Heading Projection Compensation in Substation Signal Interference Environment

Xiaolong Zhang, Tao Zhou, Jing Wang, Tao Wang, Qian Huang

State Grid Yangquan Power Supply Company, Yangquan, China
Email: zxlong1989@163.com, zhoutao@163.com, jwang@163.com, 1758484155@qq.com, 1543280889@qq.com

How to cite this paper: Zhang, X.L., Zhou, T., Wang, J., Wang, T. and Huang, Q. (2023) Personnel Localization of Real-Time Kinematic Based on Pedestrian Heading Projection Compensation in Substation Signal Interference Environment. *Journal of Sensor Technology*, **13**, 37-50.
https://doi.org/10.4236/jst.2023.132004

Received: May 10, 2023
Accepted: June 27, 2023
Published: June 30, 2023

Abstract

To address the intermittent positioning and drift of personnel positioning RTK in the high-frequency signal interference environment of substations, we propose to use IMU as the positioning compensation module of RTK and adopt the joint RTK/PDR positioning method to solve the positioning results. The heading angle is easily scattered in the pedestrian heading projection (PDR) process and the heading angles calculated from the output data of the gyroscope, accelerometer and magnetometer after denoising are input into the complementary filter for fusion. To improve the accuracy of step estimation in the PDR process, an improved step estimation model is used. For RTK/PDR data fusion, the extended Kalman filter (EKF) method is used, which helps to achieve outdoor full-scene high-accuracy positioning. The final simulation results show that RTK can be effectively compensated by PDR under the interference of high-frequency signals, and the positioning accuracy reaches 0.02 m.

Keywords

RTK, PDR, Complementary Filter, Step Size Estimation, Extended Kalman Filter

1. Introduction

In recent years, the rapid development of technology has brought location and communication technologies to a higher level, which have become an indispensable part of people's lives. When carrying out production activities, the in-

creasing demand for location services of mobile terminals makes high-precision navigation and positioning for various industries become a research hotspot at home and abroad. Some mobile terminal devices mainly rely on GNSS navigation and positioning module for positioning in the outdoor environment, and the plane accuracy can reach about 3 m in an unshielded environment [1].

Real-Time Kinematic (RTK) positioning is a branch of satellite navigation technology, which uses the carrier phase observations in the satellite signal to form differential equations and realizes real-time dynamic relative positioning between the reference station and the mobile station through rapid solution of full-period ambiguity. RTK positioning has been realized in some equipment, and the positioning accuracy is high, with no error accumulation, and can play a stable role in an unobstructed environment. It is simple, low cost and easy to operate, and is currently used in precision agriculture and high-precision navigation. The positioning accuracy has been greatly improved compared with GNSS positioning and can reach a dynamic accuracy of about 1 m.

However, in the case of obscured environment or interference from high-frequency signal sources, the GNSS of mobile terminals has a low signal-to-noise ratio and is seriously affected by multipath, leading to a rapid decline in positioning accuracy and even the phenomenon of signal lock-out, which brings a lot of inconvenience to People's Daily activities. It was found that RTK positioning technology was subject to strong signal interference from outside sources such as high-voltage power transformers when transmitting data using 4G communication links [2], leading to positioning drift problems when performing RTK positioning. The IMU (Inertial Measurement Unit) module integrated with mobile terminals collects data with a high update rate and is not affected by the external environment, helping improve positioning accuracy. However, IMU-based PDR positioning has high positioning accuracy only for a short time. For a long time, error accumulation will occur, and the combination of the advantages of RTK and PDR can realize the ideal positioning target [3]. Therefore, this paper uses the collected RTK and IMU data for processing, and uses an extended Kalman filter for fusion positioning, so as to improve the accuracy and continuity of positioning and navigation.

2. RTK Positioning Model

RTK

When RTK measurement is performed, the carrier observation and the coordinates of the base station are sent from the reference station to the working mobile station through the communication link in time, and the mobile station receives the information from the observation satellite and the reference station at the same time, and then gives the centimeter-level positioning results in real time after differential processing. The carrier phase difference model can be divided into a single difference model, double difference model and triple difference model according to the number of differences between the mobile station

and the reference station. The double-difference carrier phase observation model is based on the single-difference observation model, which detects the carrier signals of two satellites simultaneously and makes a difference between the user station reference stations and between satellite *i* and satellite *j*. The results of two differences can be obtained, compared with the single-difference model, which can further eliminate the clock difference between the user station and the reference station receivers [4] [5].

The mobile and reference stations observe satellite *i* and satellite *j* simultaneously, and the single-difference carrier phase observation for satellite *j* is given in Equation (1):

$$\phi_{ur}^{(j)} = \lambda^{-1}\left(r_u^{(j)} - r_r^{(j)}\right) + f\left(\delta t_u - \delta t_r\right) + N_u^{(j)} - N_r^{(j)} + \varepsilon_{\phi,u}^{(j)} - \varepsilon_{\phi,r}^{(j)} \tag{1}$$

The observations of satellite *i* and satellite *j* are differenced again to obtain the double-difference resultant observations with the received differential clock difference eliminated, as shown in Equation (2):

$$\phi_{ur}^{(ij)} = \phi_{ur}^{(i)} - \phi_{ur}^{(j)} \tag{2}$$

According to the above equation, the double-difference difference resultant observations can be obtained as shown in Equation (3):

$$\begin{aligned}\phi_{ur}^{(ij)} = \lambda^{-1}\left(r_u^{(i)} - r_u^{(j)} - r_r^{(i)} + r_r^{(j)}\right) + N_u^{(i)} - N_u^{(j)} \\ - N_r^{(i)} + N_r^{(j)} + \varepsilon_{\phi,u}^{(i)} - \varepsilon_{\phi,u}^{(j)} - \varepsilon_{\phi,r}^{(i)} + \varepsilon_{\phi,r}^{(j)}\end{aligned} \tag{3}$$

where, λ is the carrier wavelength, $r_r^{(i)}$ is the geometric distance between satellite *i* and the reference station *r*, $r_u^{(i)}$ represents the geometric distance between satellite *i* and the mobile station *u*, $N_u^{(i)}$ represents the whole-perimeter ambiguity of the mobile station monitoring satellite *i*, and $\varepsilon_{\phi,u}^{(i)}$ represents the carrier measurement noise of the mobile station monitoring satellite *i*. The double-difference carrier phase observation model is similar to the single- difference carrier phase observation model in principle, except that the number of unknown parameters in the equation is reduced by making the difference again, which makes the solution more convenient and further reducesthe influence of the error term. The double-difference observation model can directly eliminate the influence of the clock difference between the user station and the reference station and can eliminate the error in the electromagnetic wave transmission path.

3. PDR Positioning Model

The template is used to format your paper and style the text. All margins, column PDR uses the data from IMU combined with the position information of pedestrians at the previous moment to project the relative position of the current pedestrian, thus realizing pedestrian localization. PDR localization consists of three steps: gait detection, step length estimation, and heading angle projection. Where the accelerometer is often affected by the user's oscillation while walking,

rather than the surrounding environment or walking path. With this measurement method, the accelerometer measures little noise fluctuation and has high stability compared to other IMU sensors, so the accelerometer is used for gait detection and step length estimation.

3.1. Gait Detection

Define abbreviations and acronyms the first time they are used in the text, even the accelerometer will peak when the person is walking, and according to the periodic characteristics presented by the body when the person is walking, the peak detection method is chosen to detect the acceleration signal for footsteps. Since the pedestrian's cell phone cannot completely keep the Z-axis facing upward during walking, there will always be a certain attitude angle, and in order to improve the reliability of the acceleration in the vertical direction, the detected acceleration signal is often processed to obtain the combined acceleration [6], and the solution formula for the combined acceleration is shown in Equation (4):

$$acc(t) = \sqrt{acc_x^2 + acc_y^2 + acc_z^2} - g \tag{4}$$

where, acc_x, acc_y, acc_y, are the output data on the X, Y, and Z axes of the accelerometer, respectively, and g is the local acceleration of gravity. Combined acceleration may also exist burr noise, need to do smoothing pre-processing of combined acceleration, so use low-pass filter to process this data, the low-pass filtered combined acceleration for peak detection. In order to achieve more accurate footstep detection, the following constraints are set: 1) the peaks $peak_i$ and troughs $valley_i$ of the acceleration signal curve are found by the acceleration values of the adjacent moments before and after, and the interval between two peaks or two troughs represents one step; 2) due to the accuracy of the accelerometer and its zero bias characteristics and the peak of disturbance when the pedestrian's heel touches the ground, set the acceleration threshold σ; 3) combined with the limit speed of 0.2 s in one step of the human body, the time interval before and after the wave $T_{peak_i} - T_{peak_{i-1}}$ can be filtered to at least 0.2 s, while for general positioning, the time interval can be relaxed to 0.7 s, the constraints are shown in Equation (5):

$$\begin{cases} peak_i = (acc_i \,|\, acc_i > acc_{i-1} \,\&\&\, acc_i > acc_{i+1}) \\ valley_i = \left(acc_i \,|\, acc_i < acc_{i-1} \,\&\&\, acc_i < acc_{i+1}\right) \\ peak_i > \sigma \\ 0.2 < T_{peak_i} - T_{peak_{i-1}} < 0.7 \end{cases} \tag{5}$$

3.2. Step Size Estimation

Commonly used models for estimating step length include linear and nonlinear estimation models [7]. The linear model is only applicable to uniform and regular walking patterns and the traditional nonlinear estimation model is based on the premise that the maximum $acc_{\max}$ and minimum $acc_{\min}$ values of acceleration in the vertical direction are known for each step of the pedestrian. One of

the methods is the Weinberg step length estimation method, whose step length can be calculated using Equation (6), where K is the step length estimation parameter:

$$S = K\sqrt[4]{acc_{\max} - acc_{\min}} \tag{6}$$

In this paper, the Weinberg method is considered for step estimation in slightly complex walking patterns, and the improved step model algorithm is shown in Equation (7):

$$L = K_1 * avg\left(\Delta acc\right) * T_s + K_2\sqrt[4]{acc^{peak} - acc^{valley}} + \varepsilon \tag{7}$$

where, K_1, K_2 are the empirical parameter for step length estimation, T_s is the pedestrian step time, $avg\left(\Delta acc\right)$ represents the average acceleration between the peak and the adjacent trough, and r is the error compensation of the accelerometer. The method takes into account that the amount of change in acceleration between the peak and trough values can reflect the continuity and similarity of the pace when walking, and the estimation of the pedestrian step length is more accurate and has less error.

3.3. Heading Estimation

Traditional PDR algorithms generally use gyroscope combined with accelerometer or electronic compass to determine the heading. In this paper, Mahony complementary filtering is used to estimate heading, which has a better estimation effect by using the complementary advantages of gyroscope and electronic compass. The magnetometer output data is sliding mean filtered to perform heading estimation with accelerometer to realize the function of electronic compass. The gyroscope output data is sliding mean filtered to solve the heading angle, and the two solved heading angles are then passed through a complementary filter [8] [9] [10]. The complementary filter synthesizes a complementary result based on two inputs by assigning two reasonable weighting coefficients to the two parts of the input, which are usually both greater than zero and sum to 1. The principle of the complementary filter is shown in Equation (8):

$$\begin{aligned} &y = k_1 \cdot x_1 + k_2 \cdot x_2 \\ &k_2 + k_2 = 1 \\ &k_1, k_2 > 0 \end{aligned} \tag{8}$$

where k_1 and k_2 are the weighting coefficients of the two inputs x_1 and x_2, y is the output of the complement of x_1 and x_2 respectively. This leads to the calculation of the heading angle as

$$\varphi_k = \beta \cdot \left(\varphi_{k-1} + \omega_k \cdot \Delta T\right) + \left(1 - \beta\right) \cdot \varphi_k^{am} \tag{9}$$

where φ_k is the derived heading angle, β is the weighting factor, ω_k is the gyro output, and φ_k^{am} is the estimated heading angle from the magnetometer and accelerometer.

4. RTK/PDR Algorithm Modeling

EKF is an extended form of Kalman filtering in the nonlinear case, where the

nonlinear function is linearized by Taylor expansion, omitting the higher order terms and retaining the first order terms of the expansion, and finally the signal is filtered by approximating the state estimate and variance estimate of the system through the Kalman filtering algorithm [11] [12] [13] [14].

In the experimental test, the maximum sampling frequency of RTK is 1 Hz, and the sampling frequency of IMU is 20 Hz, because the output frequency of both is a multiplicative relationship, the output frequency of RTK is the main, and 1 s is a node to output the compensated pedestrian position. The output RTK position and PDR position are used as the input of the extended Kalman filter, and the eastward and northward positions and heading angle of the RTK are used as the state quantities, and the eastward position, northward position, heading angle and step size of the PDR solution are used as the system observations for filtering, and the filtered values are used to compensate the positioning of the RTK in the masked space, and the final RTK/PDR fusion is output localization results. Based on a comprehensive consideration of the algorithm efficiency, the extended Kalman filter is designed as follows:

The state vectors are:

$$X = \begin{bmatrix} N_k' & E_k' & \varphi_k' \end{bmatrix} \tag{10}$$

In Equation (10), N_k', E_k', φ_k', are the predicted northward position, eastward position, and heading angle, respectively. Assuming that the step and heading are consistent with a first-order Markov process, the system equation of state according to the PDR principle is

$$X_k = \begin{pmatrix} N_k' \\ E_k' \\ \varphi_k' \end{pmatrix} = \begin{pmatrix} N_{k-1} + \cos\varphi_{k-1} \\ E_{k-1} + L_k \cdot \sin\varphi_{k-1} \\ \varphi_{k-1} + \Delta\varphi \end{pmatrix} + W \tag{11}$$

In Equation (11), W is the Gaussian white noise vector of the system state equation, N_{k-1} and E_{k-1} are the fused localization result at the previous moment, L_{k-1}, φ_{k-1} is the observed value of step and heading angle at the previous moment, and $\Delta\varphi$ is the increment of heading angle estimation. The state transfer matrix A is shown in Equation (12):

$$A = \begin{pmatrix} 1 & 0 & -L_{k-1} \times \sin\varphi_{k-1} \\ 0 & 1 & L_{k-1} \times \cos\varphi_{k-1} \\ 0 & 0 & 1 \end{pmatrix} \tag{12}$$

The observation equation for this system is given by:

$$Z = \begin{pmatrix} N_k^- & E_k^- & \varphi_k & L_k \end{pmatrix}^{\mathrm{T}} + V \tag{13}$$

In Equation (13), V is the Gaussian white noise vector of the observation equation, N_k^- and E_k^- are the northward position and eastward position of the RTK at k moments, φ_k and L_k are the step size and heading angle of the observation at k moments, respectively, and the observation matrix is shown in Equation (14):

$$H = \begin{pmatrix} 1 & 0 & 0 & 0 \\ 0 & 1 & 0 & 0 \\ 0 & 0 & 0 & 1 \end{pmatrix}^{\mathrm{T}} \tag{14}$$

The initial covariance matrix of the EKF algorithm is a custom constant, but the covariance matrix of a dynamic system in a complex environment will not be fixed, and a noise feedback mechanism based on the RTK positioning results in adjacent states is used here The noise feedback mechanism based on the RTK positioning results in adjacent states is used here. where the initial position of the fusion system is given by the RTK positioning, the initial covariance matrix is P_1, the system process noise covariance matrix Q consists of the average error of each element of the east-north position, step estimate and heading angle of the PDR, and the observation noise covariance matrix consists of the average error of the RTK positioning.

$$p_1 = \begin{bmatrix} 1 & 0 & 0 \\ 0 & 1 & 0 \\ 0 & 0 & 1 \end{bmatrix}, Q = \begin{bmatrix} \delta_N^2 & 0 & 0 \\ 0 & \delta_E^2 & 0 \\ 0 & 0 & \delta_\varphi^2 \end{bmatrix}, R = \begin{bmatrix} \delta_{N_k^-}^2 & 0 & 0 & 0 \\ 0 & \delta_{E_k^-}^2 & 0 & 0 \\ 0 & 0 & \delta_L^2 & 0 \\ 0 & 0 & 0 & \delta_\varphi^2 \end{bmatrix} \tag{15}$$

where, δ_N, δ_E, δ_L, and δ_φ are the average errors of northward, eastward, step estimation, and heading angle estimation for PDR positioning, respectively. $\delta_{N_k^-}$, $\delta_{E_k^-}$ are the average error of RTK positioning north to east respectively.

After the EKF linearization and initialization is complete. The above state and observation equations are used to carry out the fusion of RTK/PDR positioning data using extended Kalman filtering.

5. RTK/PDR Algorithm Modeling

The experimental site of this time is Shanxi Province State Grid Yangquan Power Supply Company. The experimental equipment is installed as shown in **Figure 1**: The left side includes GPS wireless communication module, reference station antenna HX-CH6601A and mobile power supply, while the right side includes GPS wireless communication and inertial navigation integration module, mobile station antenna HARXON GPS500 and mobile power supply. A receiver is placed on the reference station as a reference station, which continuously observes the satellite and sends its observation data and station information to the mobile station in real time through radio transmission equipment. The mobile station receives GNSS satellite signals while receiving the data transmitted from the reference station through radio reception equipment, and then performs real-time differential operation according to the principle of relative positioning to solve the three-dimensional coordinates of the mobile station in real time and its accuracy. After power-on, the IMU acquisition device starts, the communication interface is RS422, and the baud rate is 921,600. The RTK acquisition device and attitude reference device are connected to the computer through RS422 to USB adapter. The software hdntCente developed in the laboratory on the laptop

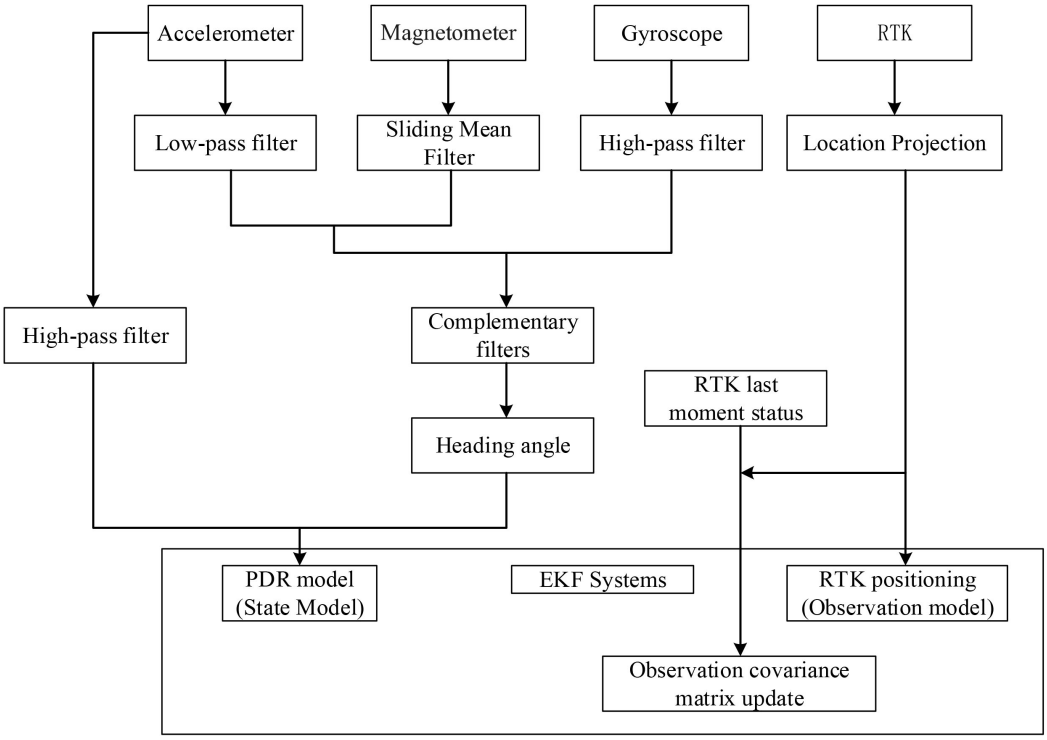

Figure 1. RTK/PDR fusion positioning algorithm flow.

computer is used to collect and store data, decode the base station observation data for RTK positioning, and obtain the RTK data set. The sampling frequency of data recording is 1 HZ. The device can achieve centimeter-level positioning accuracy. Due to the low sampling frequency of RTK, the degrees of accelerometer, gyroscope and magnetometer of IMU were separately collected by hdntCenter, and the sampling frequency was set at 20 HZ.

In this experiment, the experimenter is assumed to walk around the experimental site at a uniform speed with a step length of 0.7 m, and the right device is placed in front of the experimenter's chest as shown in **Figure 2**, and the right figure in **Figure 3**. The RTK positioning system outputs one positioning result per second and the IMU data is aligned with the RTK time, and the position solution results are shown below.

From **Figure 4**, we see that the separate RTK positioning in which a section of positioning is affected by the environment produces positioning drift, so the IMU positioning data is added to filter the RTK positioning results. The acceleration in the collected IMU output data contains high-frequency noise, which has a serious impact on the detection of gait, so the combined acceleration is low-pass filtered, and the acceleration changes as shown in Figure.

From **Figure 5**, it can be seen that after low-pass filtering, the ensemble acceleration is smoother in the time series, which effectively suppresses the high-frequency noise of the triaxial accelerometer. After that, the peak detection of the processed ensemble acceleration is performed on the gait according to the four constraints given.

Figure 2. Experimental equipment.

Figure 3. Experimental environment.

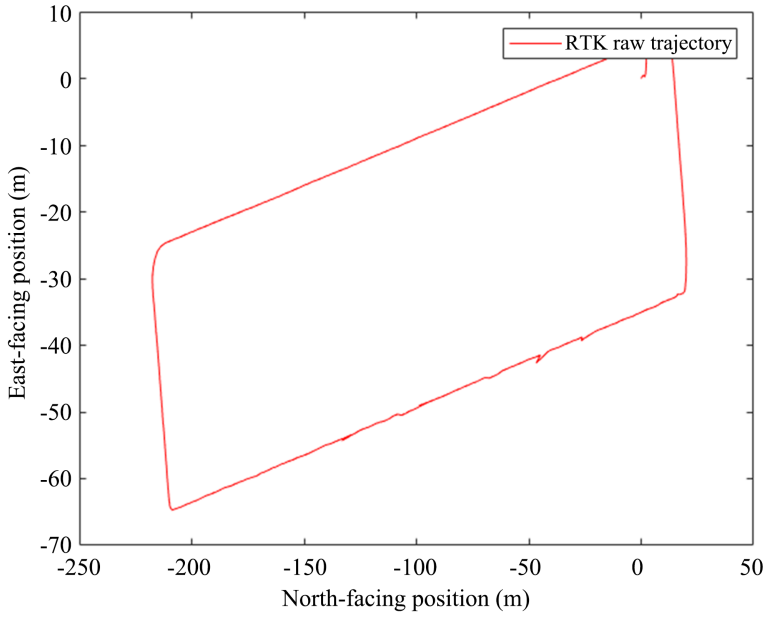

Figure 4. RTK positioning results.

It can be seen from **Figure 6** that the peak detection under the constraint is more accurate and well avoids the misidentification of the pedestrian heel touching the ground when a disturbance peak is generated. Afterwards, step estimation is performed with the improved step model algorithm and the results are shown in Figure.

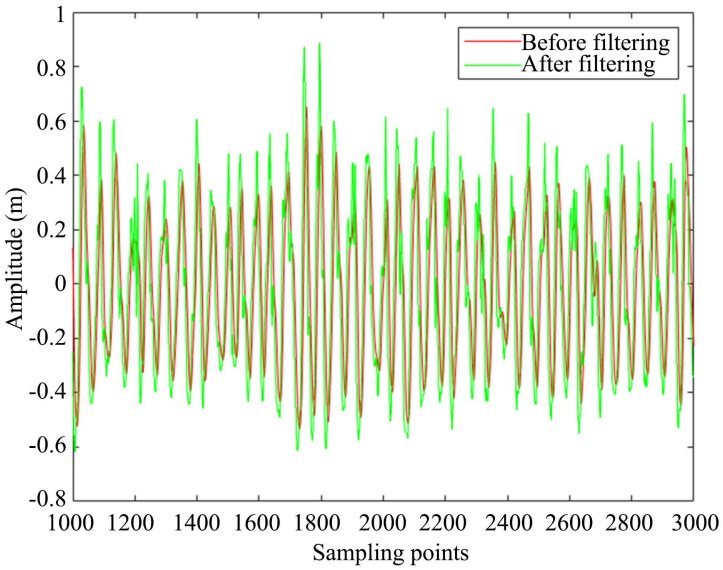

Figure 5. Acceleration comparison before and after filtering.

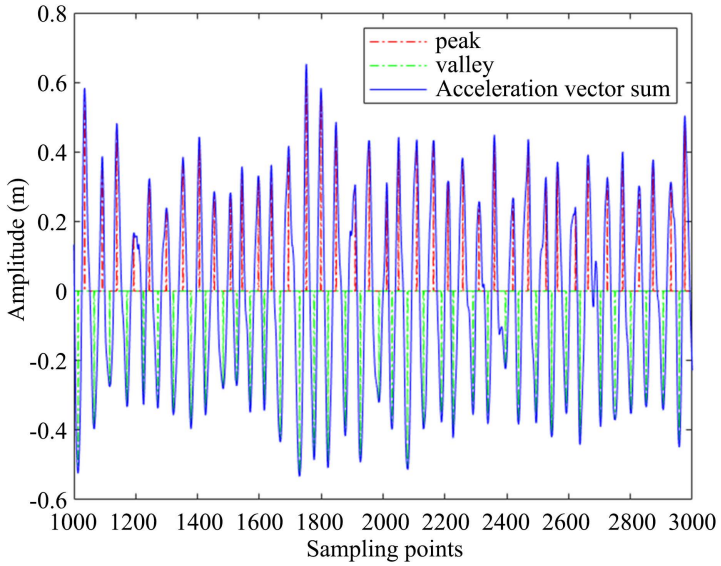

Figure 6. Peak detection.

It can be seen from Figure 7 and Table 1, the traditional weinberg algorithm, the improved step estimation algorithm has smoother fluctuations and more accurate estimation of the step length, and the error is relatively smaller in a uniform walking condition with a step length of 0.7 m.

For the combination of accelerometer and magnetometer to achieve the function of electronic compass, the gyroscope output data is high-pass filtered to solve the heading angle, the low-pass filtered accelerometer and the magnetometer output data with sliding-mean filter are solved for heading angle, and finally the heading angles of both are input into the complementary filter for fusion, and the ideal weighting coefficients are obtained experimentally, and the results obtained are shown in Figure 8.

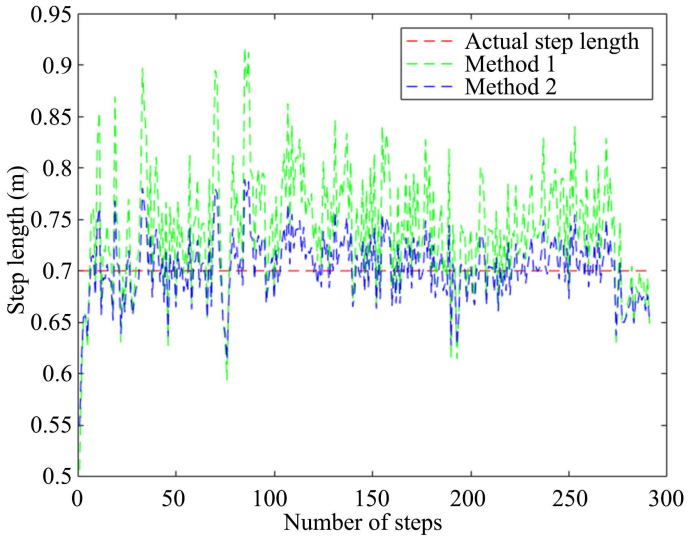

Figure 7. Step estimate.

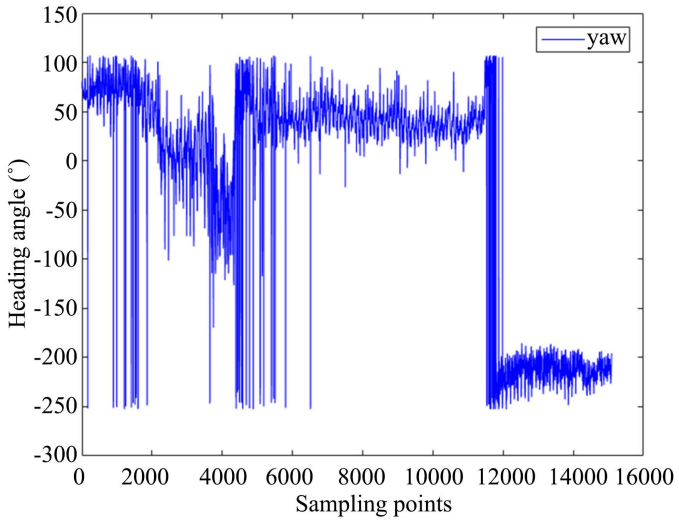

Figure 8. Electronic compass heading angle.

Table 1. Comparison of step estimation errors.

	Estimated mean value f step size	Real step length	Mean value of step error
Method 1	0.72	0.7	0.02
Method 2	0.88	0.7	0.11

It can be seen that the heading angle solved by the accelerometer and magnetometer is affected by the magnetic field, and noise is generated in the disturbed region of the magnetic field, so the principle of complementary filtering is used to add the heading angle solved by the gyroscope, and two reasonable weighting coefficients are assigned to the two parts of the input to obtain the ideal heading angle results. (**Figure 9**)

The extended Kalman filter is used for data fusion of the RTK and PDR positioning results, and the filtered value is used to compensate the positioning of RTK in the shelter space. Noise variance of PDR system walking direction is (0.65˚/step), noise variance of step size is (0.07 m/step), and positioning error of RTK system is (<2 cm). The filtered results are shown as follows:

As can be seen in **Figure 10**, in a section on personnel positioning, the positioning accuracy of RTK drifts indefinitely and even decreases to the meter level due to the high-frequency signal interference generated by high-voltage power transformers. IMU, as a fully autonomous navigation method, can achieve high-precision positioning of personnel in the case of short-term accuracy degradation of RTK, and the positioning can reach the centimeter level.

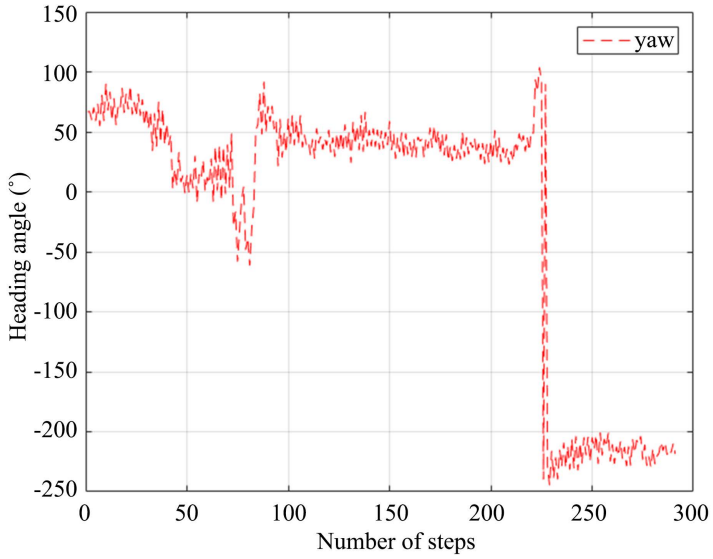

Figure 9. Course angle after complementary filtering.

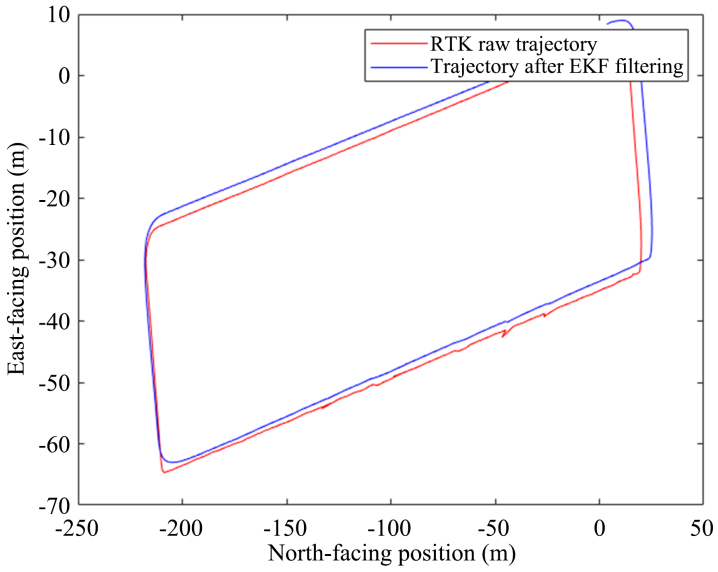

Figure 10. EKF filtering comparison results.

6. Conclusions

The template in this paper, an RTK/PDR filter fusion algorithm, is proposed to address the problem of RTK positioning drift in the obscured environment, which effectively solves the problem of low and discontinuous RTK positioning accuracy in an environment with weak or even out-of-lock GNSS signals under the influence of the environment, using GNSS observations and IMU data from mobile devices.

The experimental results show that the mobile device RTK can achieve centimeter-level positioning in a good observation environment, making it feasible to achieve high-precision positioning. For positioning under environmental occlusion space, the IMU data can compensate well for the RTK positioning drift. The adopted PDR heading estimation adopts a complementary filtering algorithm, which improves the accuracy and anti-interference capability of the traditional heading estimation algorithm. The fusion algorithm uses Kalman filtering, which combines the advantages of RTK and PDR positioning. PDR provides continuous positioning results under a poor observation environment, which compensates for the weakness of RTK anti-interference capability. It can basically meet the daily navigation and positioning needs of the general public.

Acknowledgements

This work was funded by the Science and Technology Project of State Grid Shanxi Electric Power Company, "Research and application of key technologies of elastic fusion security operation in digital region based on 5G and deep learning," 5205C0220001.

Conflicts of Interest

The authors declare no conflicts of interest regarding the publication of this paper.

References

[1] Zhao, S., Chen, Y.M. and Farrell, J.A. (2016) High-Precision Vehicle Navigation in Urban Environments Using an MEM's IMU and Single-Frequency GPS Receiver. *IEEE Transactions on Intelligent Transportation Systems*, **17**, 2854-2867. https://doi.org/10.1109/TITS.2016.2529000

[2] Zhang, Q., *et al.* (2022) A Smartphone RTK Algorithm Based on Velocity Constraint. *Proceedings of the* 13*th Annual China Satellite Navigation Conference*. Beijing, 26 April 2022, 437-450. https://doi.org/10.1007/978-981-19-2588-7_41

[3] Li, W.Y., *et al.* (2021) Feature-Aided RTK/LiDAR/INS Integrated Positioning System with Parallel Filters in the Ambiguity-Position-Joint Domain for Urban Environments. *Remote Sensing*, **13**, Article 2013. https://doi.org/10.3390/rs13102013

[4] Liu, F., *et al.* (2019) An Indoor Localization Method for Pedestrians Base on Combined UWB/PDR/Floor Map. *Sensors*, **19**, Article 2578. https://doi.org/10.3390/s19112578

[5] Li, L.H., Yuan, Y.B. and Zhang, P.F. (2023) On Low-Cost GNSS Observables under

Different Grades of Antennas: Receiver-Related Biases and RTK Results. *Measurement*, **214**, Article 112771. https://doi.org/10.1016/j.measurement.2023.112771

[6] Kim, K.S., and Shin, Y. (2021) Deep Learning-Based PDR Scheme That Fuses Smartphone Sensors and GPS Location Changes. *IEEE Access*, **9**, 158616-158631. https://doi.org/10.1109/ACCESS.2021.3130605

[7] Davidson, P. and Piché, R. (2017) A Survey of Selected Indoor Positioning Methods for Smartphones. *IEEE Communications Surveys and Tutorials*, **19**, 1347-1370. https://doi.org/10.1109/COMST.2016.2637663

[8] Zun, N., *et al.* (2022) An Algorithm to Assist the Robust Filter for Tightly Coupled RTK/INS Navigation System. *Remote Sensing*, **14**, Article 2449. https://doi.org/10.3390/rs14102449

[9] Valenti, R.G., *et al.* (2015) Keeping a Good Attitude: A Quaternion-Based Orientation Filter for IMUs and MARGs. *Sensors*, **15**, 19302-19330. https://doi.org/10.3390/s150819302

[10] Gu, S.F., *et al.* (2022) Integration of Multi-GNSS PPP-RTK/INS/Vision with a Cascading Kalman Filter for Vehicle Navigation in Urban Areas. *Remote Sensing*, **14**, Article 4337. https://doi.org/10.3390/rs14174337

[11] Li, Z.K., *et al.* (2020) Wifi/PDR Integrated Navigation with Robustly Constrained Kalman Filter. *Measurement Science and Technology*, **31**. https://doi.org/10.1088/1361-6501/ab87ea

[12] Sun, M., *et al.* (2020) Indoor Positioning Tightly Coupled Wi-Fi FTM Ranging and PDR Based on the Extended Kalman Filter for Smartphones. *IEEE Access*, **8**, 49671-49684. https://doi.org/10.1109/ACCESS.2020.2979186

[13] Cui, Y., *et al.* (2020) Integrated WiFi/MEMS Indoor Navigation Based on Searching Space Limiting and Self-calibration. *Arabian Journal for Science and Engineering*, **45**, 3015-3024. https://doi.org/10.1007/s13369-019-04249-z

[14] Lee, J.S. and Huang, S.M. (2019). An Experimental Heuristic Approach to Multi-Pose Pedestrian Dead Reckoning without Using Magnetometers for Indoor Localization. *IEEE Sensors Journal*, **19**, 9532-9542. https://doi.org/10.1109/JSEN.2019.2926124